Towards Automated Stimulation Parameter Titration for Deep Brain Stimulation: A Connectivity-based Approach

Undergraduate Research Thesis

Presented in partial fulfillment of the requirements for graduation
with honors research distinction in Biomedical Engineering at The Ohio State University

Author: Qinwan Rabbani

Project Advisor: Dr. Vibhor Krishna, Department of Neurological Surgery

The Ohio State University
April 2018

ACKNOWLEDGEMENTS

Vibhor Krishna, MBBS
Department of Neurological Surgery, Center for Neuromodulation, The Ohio State University Wexner Medical Center

Francesco Sammartino, MD
Department of Neurological Surgery, Center for Neuromodulation, The Ohio State University Wexner Medical Center

Mark Ruegsegger, PhD
Department of Biomedical Engineering, The Ohio State University

ABSTRACT

Deep brain stimulation (DBS) is an effective surgical treatment for drug-resistant neurological movement disorders like Parkinson's disease and essential tremor. However, as the complexity of DBS leads increases, the standard method for stimulation parameter titration will become increasingly challenging and definitive parameter search more time-consuming. For this reason, we proposed a connectivity-based approach using patient-specific cortical connectivity for predicting clinical outcome, and designed our study to serve as a proof-of-concept for automating stimulation parameter titration. Specifically, we obtained brain images from a cohort of 24 Parkinson's patients implanted with subthalamic nucleus (STN) DBS and calculated the differences in connectivity to cortical regions in the whole brain associated with specific clinical observations sorted by clinical outcome: "Improvement" or "Side Effect." We then reduced the number of cortical regions using reverse sequential feature selection before training a linear support vector machine (SVM) using 10-fold cross validation to classify clinical observations by clinical outcome using their associated differences in cortical connectivity. This SVM was then used to predict the most efficacious contact for each DBS lead, as well as the most efficacious voltage at each contact on each lead. The SVM achieved an overall classification error of 10.99%, and predicted the most efficacious contact with an average absolute deviation of 0.89, 1.17 and 1.08 contacts and 0.77, 1.10 and 1.21 V from the initial, 1 year and final stimulation parameter settings respectively. Additionally, it was found that 44.1% of the contacts were non-efficacious with 6 leads being entirely non-efficacious. Though these results are relatively modest, together they suggest that our metric is informative for predicting clinical outcome and narrowing down stimulation parameters. In the future, we hope to refine our algorithm to improve performance considerably. Our study serves as a useful first step towards the automation of stimulation parameter titration for DBS surgery.

INTRODUCTION

Deep Brain Stimulation

Deep brain stimulation (DBS) is an effective surgical treatment method for drug-resistant neurological movement disorders, though its potential is also being explored for various other neurological and psychological disorders (Miocinovic et al. 2013). Specifically, DBS is currently an FDA-approved therapy for essential tremor and Parkinson's disease, and has a humanitarian device exemption for dystonia and obsessive-compulsive disorder (OCD) (Miocinovic et al. 2013). However, despite the great success DBS has shown in treating these disorders, its exact therapeutic mechanisms are unclear.

The DBS system typically consists of one lead for each cerebral hemisphere with 4 stimulating contacts each, which can be placed either unilaterally (ie: in a single hemisphere) or bilaterally (ie: in both hemispheres) (Miocinovic et al. 2013). Each of the contacts can be stimulated individually (unipolar stimulation) or in combination (multipolar stimulation) (Miocinovic et al. 2013). By testing multiple stimulation parameters, the most effective set of parameters can be found by balancing therapeutic effects while minimizing side effects. A typical DBS implant setup is shown in Figure 1:

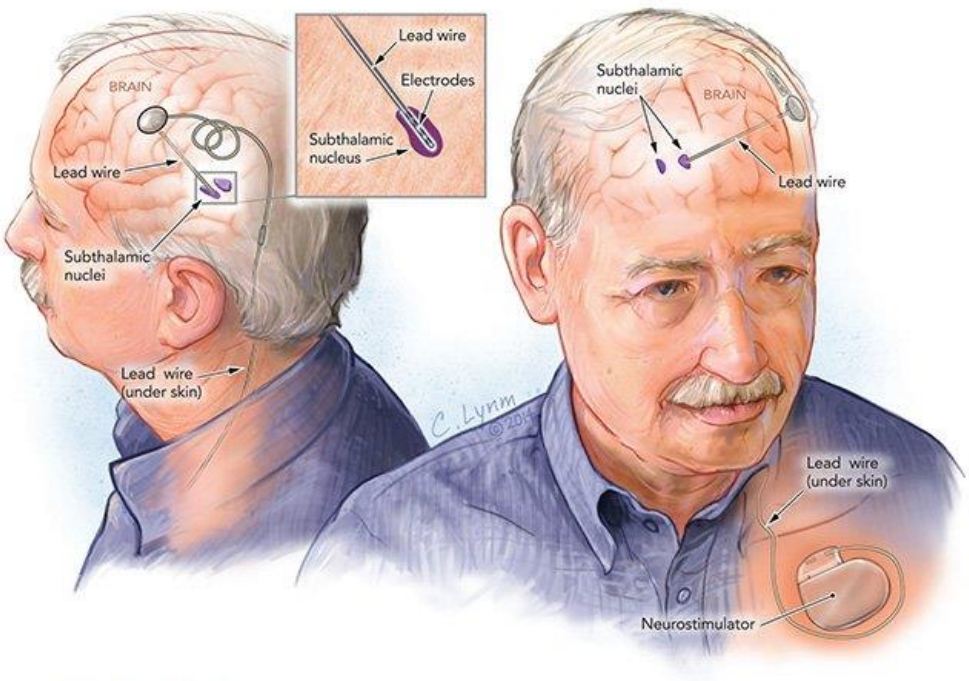

Figure 1: Each DBS lead is inserted through an opening in the skill deep into the brain tissue terminating in a target site, such as the subthalamic nucleus (STN). Patients can be implanted either unilaterally (one lead, single hemisphere) or bilaterally (two leads, both hemispheres) ("Deep Brain Stimulation for Parkinson's Disease" 2018). The lead(s) are then powered by a wire routed to a portable neurostimulator under the skin in the chest area ("Deep Brain Stimulation for Parkinson's Disease" 2018).

Deep Brain Stimulation for Parkinson's Disease

Parkinson's disease is a progressive neurodegenerative disorder that manifests primarily as bradykinesia (a slowing of movements), rigidity (stiffness) and tremors (uncontrolled shaking of the limbs) due to a depletion of dopamine (Kalia and Lang 2015). Though dopaminergic treatments like levodopa are effective in reducing these symptoms, patients may develop side effects (ie: dyskinesia) or fluctuations in the clinical efficacy. DBS is an adjunct to medical treatment for advanced Parkinson's patients with excellent long-term clinical efficacy (Schuepbach et al. 2013). The most common targeting sites include the subthalamic nucleus (STN) and globus pallidus internus (GPi) (Williams, Foote, and Okun 2014). Because Parkinson's DBS is one of the most commonly performed DBS procedures, we applied our algorithm first to this disorder, though it is could arbitrarily be extended to other neuropsychological disorders as well.

Stimulation Parameter Titration

Once the DBS leads have been implanted in the target regions, the next step is to test different stimulation parameters in what is known as programming or stimulation parameter titration. The specific parameters that can be optimized include the optimal electrode contact(s), stimulation voltage(s), pulse width and frequency, and can be visualized via their corresponding volume of tissue activation(s) (VTA) (Miocinovic et al. 2013). An illustration of the VTA resulting from stimulation is shown in Figure 2:

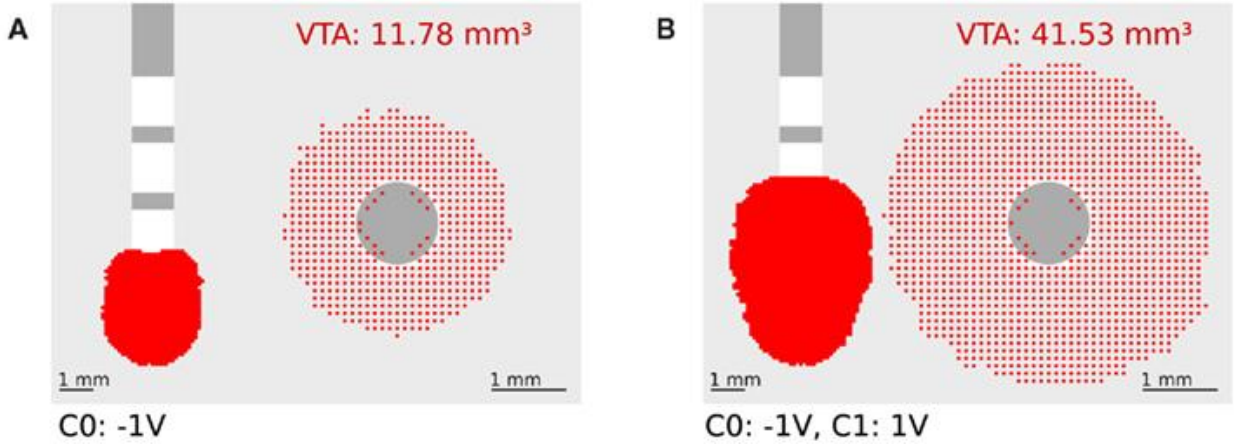

Figure 2: The volume of tissue activation (VTA) can be modeled by simulating the interaction between the electrical field generated by the lead and the surrounding tissue (Buhlmann et al. 2011). Stimulation can be done either in a monopolar (single contact, left) or multipolar fashion (multiple contacts, right) in order to stimulate different areas of the surrounding tissue (Buhlmann et al. 2011).

Traditionally, stimulation parameter titration has been done through a systematic, trial-and-error process in which each contact is tested independently with varying sets of parameters, while noting clinical improvements and side effects (Picillo et al. 2016a, 2016b). This process most typically takes anywhere from 30 to 120 minutes per DBS lead (Ondo, Bronte-Stewart, and DBS Study Group 2005). Though the final stimulation parameters are selected by the end of the initial programming session, these parameters may require adjustment over successive clinical visits (Miocinovic et al. 2013). However, this method for stimulation parameter selection will become more challenging, and definitive parameter search more time-consuming, as more complex lead setups with higher contact counts and directional stimulation capabilities become more common

(Schüpbach et al. 2017; Anderson et al. 2018). For this reason, automated methods for stimulation titration incorporating brain connectivity are needed.

Tractography for Deep Brain Stimulation

Though the exact therapeutic mechanisms of DBS are still unclear, the leading hypothesis is that the electrical stimulation of neural elements, neuronal cell bodies and axons, surrounding the DBS lead has local and downstream network-level effects resulting in clinical efficacy (Okun and Oyama 2013). These network-level effects are likely mediated primarily through the white matter tracts projecting from and surrounding the target site, which is in alignment with previous in vitro studies (Okun and Oyama 2013; Nowak and Bullier 1998). These white matter tracts can be studied in vivo using diffusion tensor imaging (DTI), by modeling the diffusion properties of water molecules in the brain (Assaf and Pasternak 2008). Tractography is the computational reconstruction method which utilizes the diffusion information from DTI to infer the trajectories of these white matter pathways and thus the underlying structural connectivity in the brain (Maier-Hein et al. 2017). Because clinical observations commonly appear after incremental changes in stimulation parameters, by modeling the differences in stimulation volume, it may be feasible to study the changes in structural connectivity associated with these stimulation-induced clinical observations using tractography. We hypothesize that the additional cortical connectivity associated with stimulation adjustment may be involved in the appearance of stimulation-induced clinical effect.

Support Vector Machines

The support vector machine (SVM) is a common machine learning method that has been applied successfully to a variety of classification problems (Salcedo-Sanz et al. 2014). Mathematically, the SVM is defined as maximum margin classifier, the goal of which is to identify the hyperplane(s) within the high dimensional feature space that maximally segregates the class(es) (Salcedo-Sanz et al. 2014). These hyperplanes then serve as the decision boundaries by which the trained SVM classifies an observation as one class or another (Salcedo-Sanz et al. 2014). Because of its definition, the output of an SVM will always correspond to the mathematically optimal decision boundaries for the given

training data (Salcedo-Sanz et al. 2014). The SVM therefore is a reasonable method by which to consistently determine whether specific features are predictive of a classification. An illustration of the principle by which SVMs classify data is shown in Figure 3:

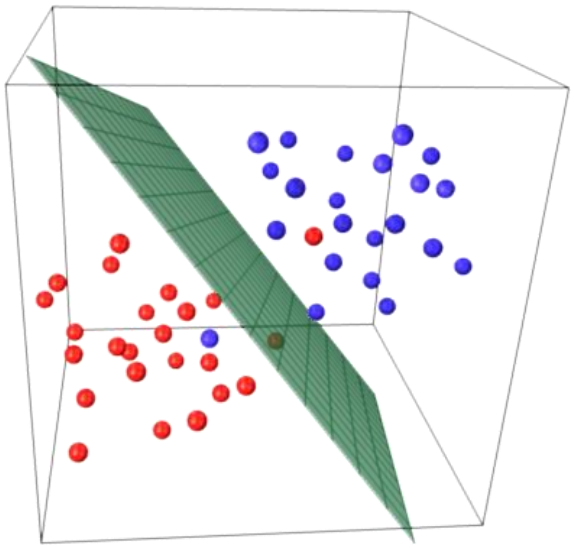

Figure 3: Illustration of linear SVM Classification. The purpose of the SVM is to find the optimal decision boundary in feature space between classes, while maximizing the margin of separation and minimizing misclassification error. Though illustration shows this principle in 3-dimensional space, this can be arbitrarily extended to higher dimensional feature spaces as well (which cannot as easily be visualized).

OBJECTIVE

In its current state, stimulation parameter titration is a systematic, trial-and-error method, which can be rather time-consuming for both the patient and clinician. Though this traditional method has been highly successful, it may become more challenging and time-consuming as the complexity of DBS lead setups increases. For this reason, we propose a connectivity-based approach using patient-specific cortical connectivity to predict specific stimulation settings with a high likelihood for good outcome. Additionally, we aim to use this study as a proof-of-concept for a connectivity-based approach for automated stimulation parameter titration.

METHODS

Image Acquisition

In this study, we retrospectively examined a cohort of 24 Parkinson's patients implanted with STN DBS at the Center for Neuromodulation in the Ohio State Wexner Medical Center. All patients signed informed consent, and the study was approved by the Ohio State University Wexner Medical Center Ethics Board. Preoperatively, all patients underwent both T1 (1mm isovoxel, MPRAGE) and diffusion-weighted imaging (DTI, 64 directions, 2mm isovoxel, whole-brain acquisition) on a Philips Ingenia CX 3 Tesla magnet, using a padded 32 channel bird cage coil to minimize discomfort and head motion. Postoperatively, all patients underwent a CT scan of the head 4-6 weeks after implantation of DBS electrodes. T1-weighted MR images were used for visualizing patient-specific anatomy. DTI images were used for estimating whole-brain diffusivity. CT images were used to localize the final location of the implanted DBS leads using the electrode artifacts. Together, these images formed the basis of our stimulation modeling and whole-brain connectivity analysis. Examples of each image acquisition are shown in the figures following:

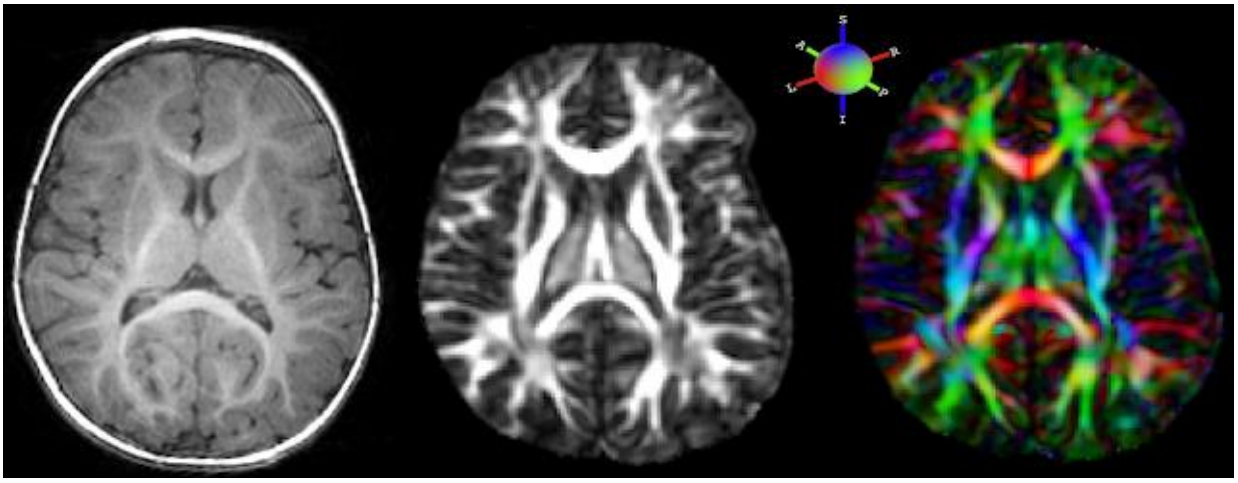

Figure 4: Diffusion tensor image (DTI) displayed as a raw T1-weighted MR image (left), along with corresponding fractional anisotropy (FA) maps in greyscale (middle) and color (right) (Tromp 2009). Fractional anisotropy is a method which quantifies the relative length of each diffusion tensor in comparison to its width, or analogously quantifies the fraction of the tensor that is non-isotropic (Tromp 2009). This provides a measure of the direction of diffusivity of water molecules in the brain, which move preferentially along white matter tracts but more randomly within gray matter (Tromp 2009).

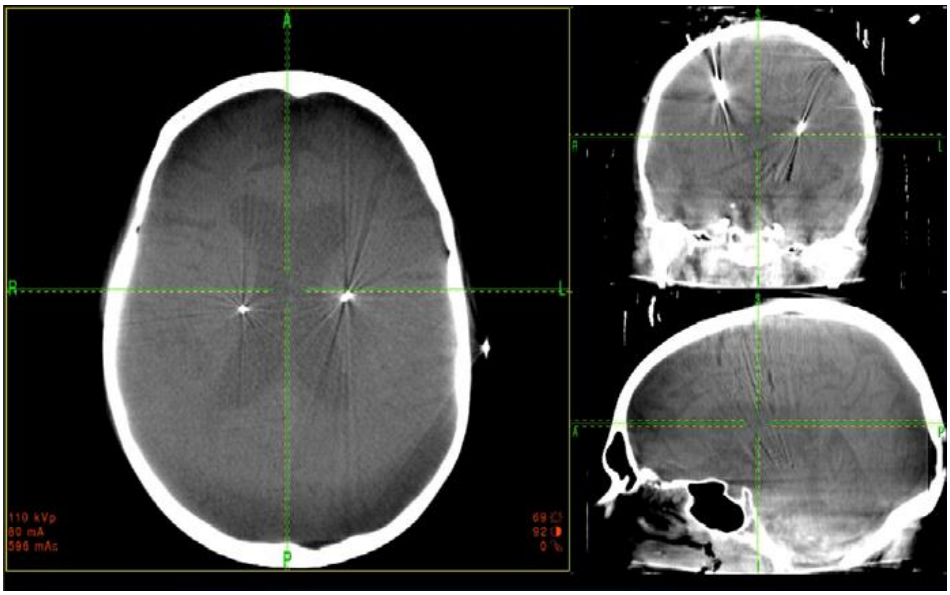

Figure 5: The metallic contacts of the DBS lead can be seen in the postoperative CT images by their electrode artifacts (Zhang 2013). These artifacts can be used to localize the final location of the contacts for use in later stimulation modeling.

Stimulation Parameter Titration

During stimulation parameter titration, the voltage was varied for each individual contact in a step-wise manner while maintaining a frequency of 130 Hz and pulse width of 90 μs. Though one of the cases did include bipolar stimulation, the majority of the cases were monopolar. This resulted in 355 unique voltage changes in 38 leads (14 bilateral, 2 right, 8 left) across the entire 24-patient cohort. For each voltage change, clinical effects were noted and classified into "Improvement" or "Side Effect" (119 and 236 voltage changes respectively) in 15 clinical domains. These domains were as follows: rigidity (domain 1), bradykinesia (domain 2), tremor (domain 3) improvement; and sensory (domain 4), motor (domain 5), limbic (domain 6), dyskinesia (domain 7), eye deviations (domain 8), gait (domain 9), dizziness (10), other (11), dystonia (12), sweating (domain 13), fatigue (domain 14) and vision changes (domain 15) side effect.

Image Processing

Images were preprocessed using our custom, MATLAB-based DBSProcessor pipeline, that interfaced with standard neuroimaging software packages such as FSL and Lead-DBS

("MATLAB - MathWorks" 2018; Jenkinson et al. 2012; Horn and Kühn 2015). The CT, DTI and T1-weighted MR images of 24 patients were first deidentified then imported and converted from DICOM to NIfTI format for analysis. The DTI images were pre-processed for motion artifact correction (eddy_correct, FSL suite), and run through DTIFIT (DTIFIT, FSL suite) to estimate the diffusion tensors and BEDPOSTX (bedpostx, FSL suite) for Bayesian estimation of the diffusion parameters at each voxel. Then, the CT and T1-weighted MR images were co-registered and normalized to a high-resolution, 0.5mm MNI-ICBM 152 group brain template from the ICBM 2009b Nonlinear Asymmetric atlas using Lead-DBS's ANTs implementation (Fonov et al. 2009). The leads were then localized (and visually confirmed) and each unique VTA pair associated with the voltage changes calculated using Lead-DBS. A nonlinear transform was then calculated from diffusion to ICBM-MNI template space (FNIRT, FSL suite).

To estimate patient-specific connectivity, whole-brain probabilistic tractography using PROBTRACKX (probtrackx2, FSL suite) was then performed between each voxel in each patient's native diffusion space. The settings included the omatrix2 option, 100 samples per voxel, a curvature threshold of 0.2, a maximum number of steps per sample of 2000, a step length of 0.5 mm, a subsidiary fiber volume threshold of 0.01 and a loopback check. The connectivity matrix generated by probabilistic tractography was then used to infer the strength of connectivity from each VTA to 360 distinct cortical regions segmented by hemisphere. The change in connectivity between each VTA pair was then statistically thresholded to isolate significant connectivity changes from baseline (Glasser et al. 2016). The resulting "differential" cortical connectivity feature vectors were then used in further analysis.

Stimulation Parameter Prediction

After generating the connectivity data, we then trained a linear SVM (fitcsvm, MATLAB toolbox) to classify the changes in cortical connectivity corresponding to particular clinical voltage changes by clinical outcome as "Improvement" or "Side Effect." In order to ensure a parsimonious model, the 360 cortical regions used previously were narrowed down to only the most predictive regions using reverse sequential feature selection. This optimal set of

features was then used in final training. Finally, 10-fold cross validation with 250 10-fold iterations was used to ensure the generalizability of our model, with the overall error on the entire dataset serving as the final performance metric for our linear SVM classifier. Next, the most efficacious contacts for each lead was predicted using the SVM predictions, by determining the highest efficacious voltage predicted before encountering side effects. The center of mass of the contacts was then computed for each prediction, and compared to that of the initial, 1 year and final stimulation parameter settings. Similarly, the predicted voltage was likewise compared to the that of the initial, 1 year and final stimulation parameter settings. The averages of the absolute deviations were then taken to determine overall performance of our algorithm for contact and voltage prediction.

RESULTS

Selected Features

The final result of reverse sequential feature selection was 156 cortical regions that were most predictive of clinical outcome. These cortical regions are listed in Table 1:

Hemisphere	Cortical Regions
Right	V6, V4, 4, 3b, PEF, RSC, POS2, V7, IPS1, V3B, LO2, PIT, PSL, 7Pm, 23d, v23ab, d23ab, 5m, 5L, 24dv, 6ma, 7Am, VIP, 2, 6d, 6v, a24pr, a24, 10r, 8Ad, 10d, 45, a47r, IFJa, IFJp, IFSp, 11l, 13l, 47s, LIPd, 43, OP4, PFcm, PoI2, TA2, FOP4, FOP3, H, ProS, STGa, PBelt, STSdp, STSvp, TGd, TE1a, TE2a, TF, PH, TPOJ2, IP1, IP0, PF, PFm, V6A, VMV1, VMV3, PHA2, V4t, V3CD, VMV2, 31pd, 31a, VVC, FOP5, MBelt, LBelt, A4, STSva
Left	55b, 5mv, p24pr, 8BM, 8Av, 9p, 44, IFSa, 10v, OP1, RI, AAIC, AIP, PFop, PGs, LO3, PoI1, p24
Both	MIP, p32, 8C, 6r, a9-46v, 9-46d, a10p, i6-8, OP2-3, MI, FOP1, EC, PreS, A5, PHA1, TE1p, TPOJ1, TPOJ3, DVT, PGp, IP2, PGi, FST, 25, pOFC, Ig, p10p, TGv, TE1m, a32pr

Table 1: Most predictive cortical regions as sorted by hemisphere.

These regions were then translated into their corresponding cortical areas, then sorted by their primary cortical functions. The sorted cortical areas are listed in Table 2:

Primary Function	Cortical Areas
Motor	PFC, Broca's Area, PMC, SMA, M1, POS
Sensory	5M, 24', MIP, S1, 5, 5L
Visual	FEF, AIP, DVT, PG, FST, LO, V3, V4, V6, V7, PEF, IPS, PIT, 7, 7A, VIP, PH, VMV, VVC
Limbic	Insular Cortex, Subgenual Area, OFC, TG, 25
Other	55b, 32, 32', 8A, IFS, OP, Entorhinal Cortex, Presubiculum, A1, A4, A5, PHA1, TPOJ, 24, RSC, PSL, 23, 47, IFJ, 11, 13, 43, 40, Hippocampus, Prosubiculum, STG, STS, TF

Table 2: Cortical areas comprising the predictive cortical regions as sorted by primary neurological function.

Prediction Results

A linear SVM was trained (fitcsvm, MATLAB toolbox) to classify VTA changes using their corresponding "differential" cortical connectivity feature vectors to the aforementioned 156 cortical regions using 10-fold cross validation ("MATLAB - MathWorks" 2018). The best performing SVM model was then used to predict clinical outcome for all 355 VTA changes. This resulted in an overall classification error of 10.99%.

The SVM was then used to classify the most efficacious contacts based on the contacts that displayed the highest voltage associated with improvement before encountering any side effects. This prediction was then compared to the initial, one year and final stimulation parameter settings. The predictions were found to deviate on average from the experimentally-chosen contacts and voltages by 0.89, 1.17 and 1.08 contacts and 0.77, 1.10 and 1.21 V respectively. Additionally, it was found that 44.1% (67 out of 152) of the contacts predicted were non-efficacious (ie: 0 V prediction) with 6 leads being entirely non-efficacious. These results are summarized in Figure 6 and Table 3 following:

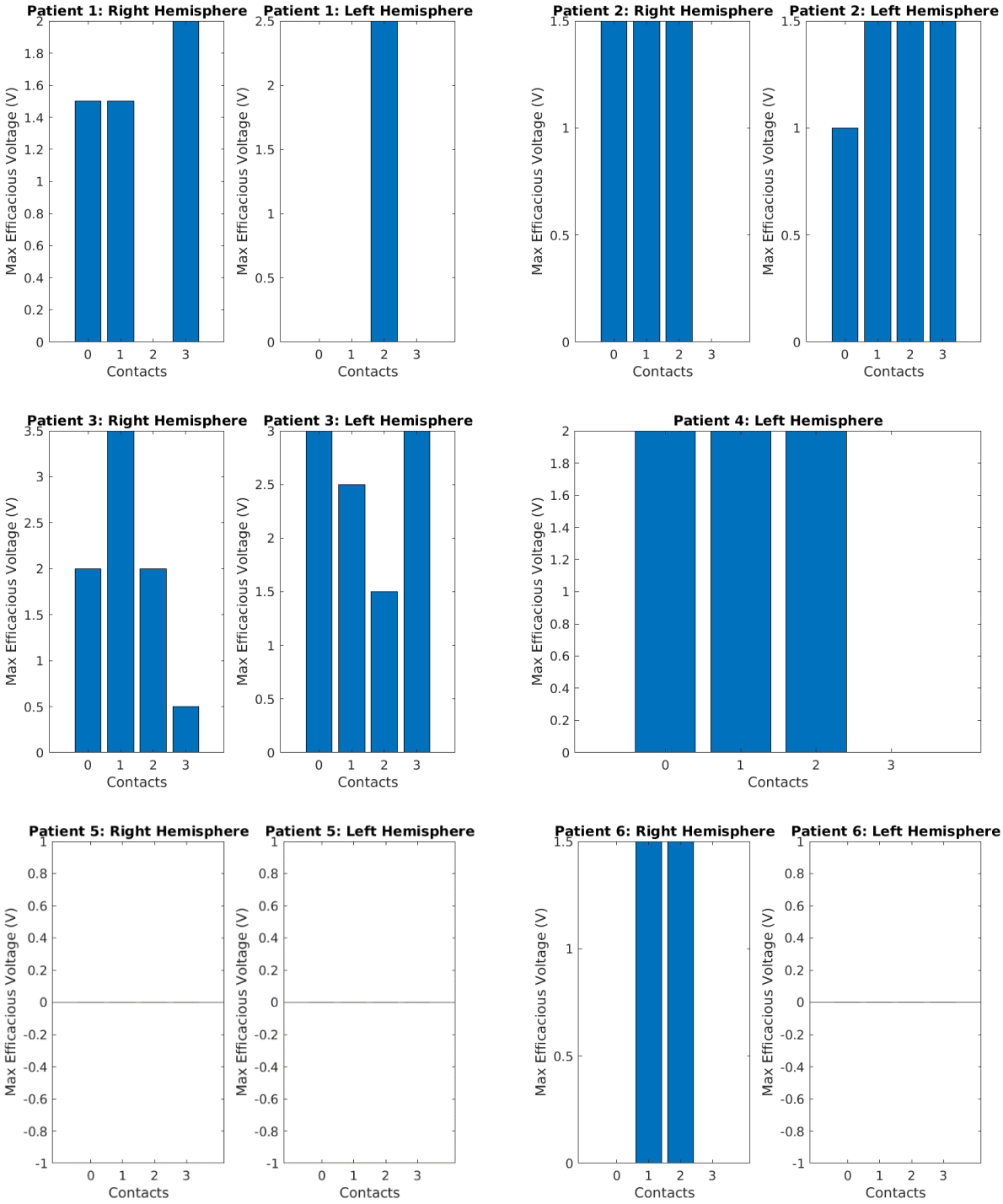
Patient 1: Right Hemisphere
Patient 1: Left Hemisphere
Patient 2: Right Hemisphere
Patient 2: Left Hemisphere
Patient 3: Right Hemisphere
Patient 3: Left Hemisphere
Patient 4: Left Hemisphere
Patient 5: Right Hemisphere
Patient 5: Left Hemisphere
Patient 6: Right Hemisphere
Patient 6: Left Hemisphere
Max Efficacious Voltage (V)
Contacts

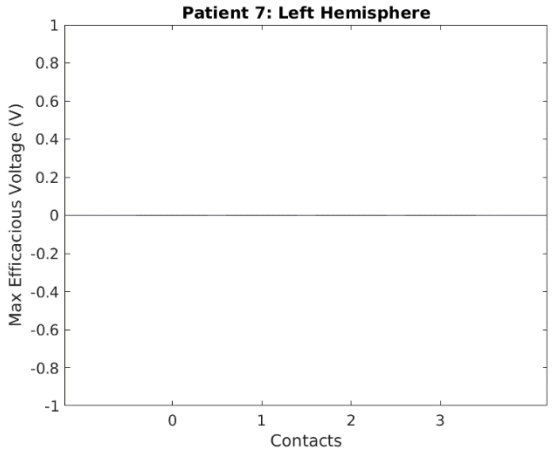
Patient 7: Left Hemisphere
Max Efficacious Voltage (V)
Contacts

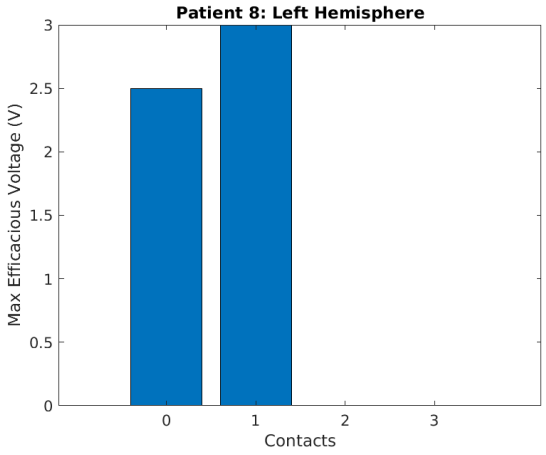
Patient 8: Left Hemisphere
Max Efficacious Voltage (V)
Contacts

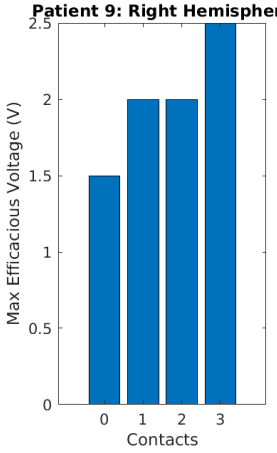
Patient 9: Right Hemisphere
Max Efficacious Voltage (V)
Contacts

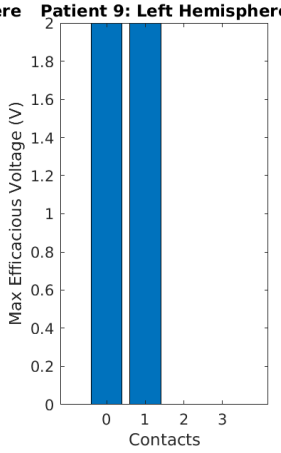
Patient 9: Left Hemisphere
Max Efficacious Voltage (V)
Contacts

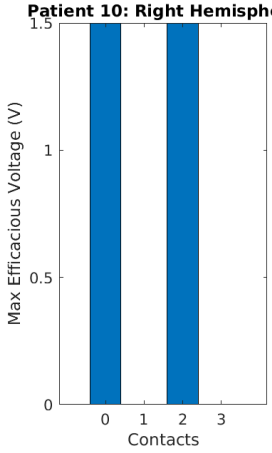
Patient 10: Right Hemisphere
Max Efficacious Voltage (V)
Contacts

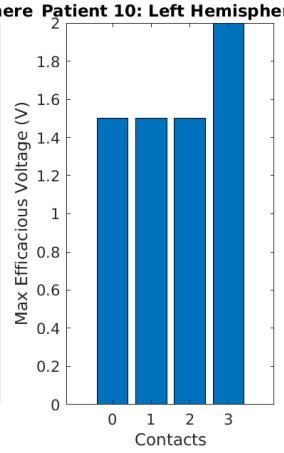
Patient 10: Left Hemisphere
Max Efficacious Voltage (V)
Contacts

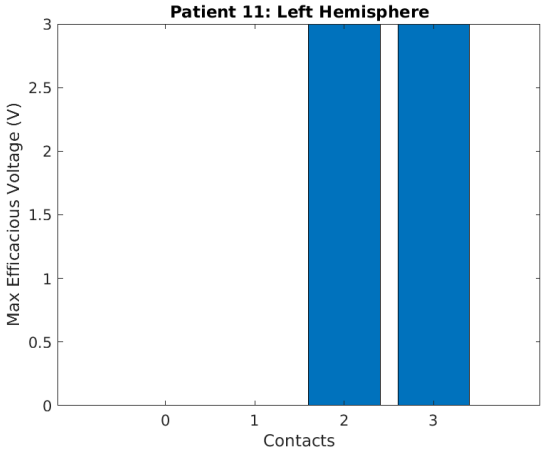
Patient 11: Left Hemisphere
Max Efficacious Voltage (V)
Contacts

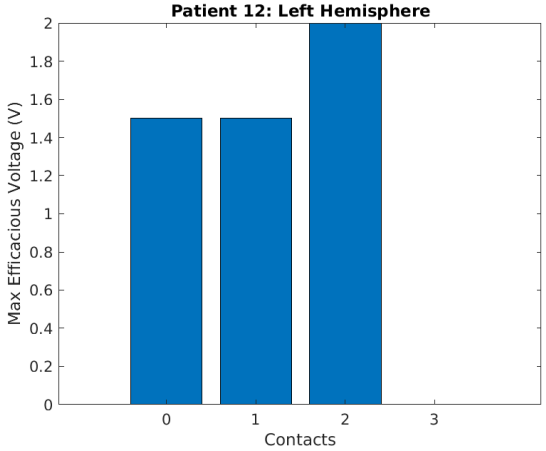
Patient 12: Left Hemisphere
Max Efficacious Voltage (V)
Contacts

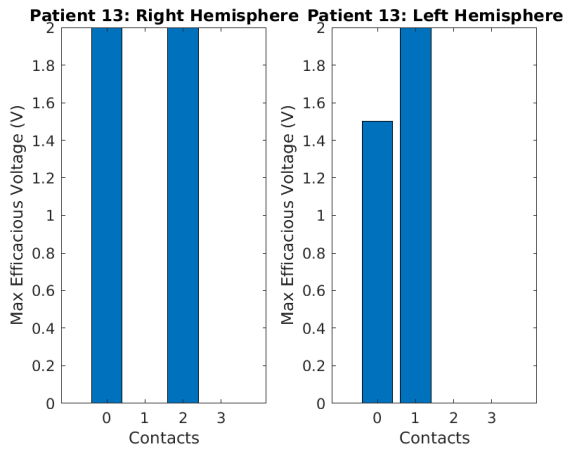
Patient 13: Right Hemisphere
Max Efficacious Voltage (V)
Contacts

Patient 13: Left Hemisphere
Max Efficacious Voltage (V)
Contacts

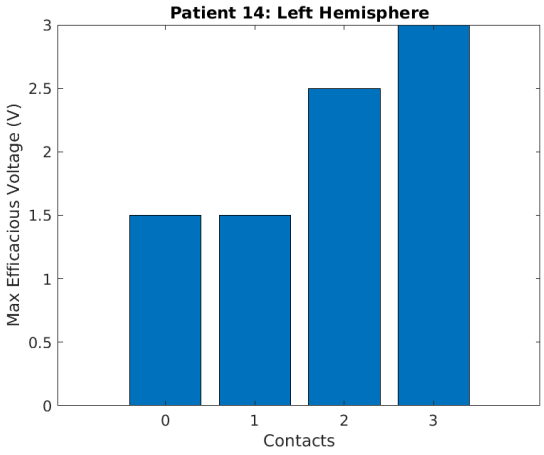
Patient 14: Left Hemisphere
Max Efficacious Voltage (V)
Contacts

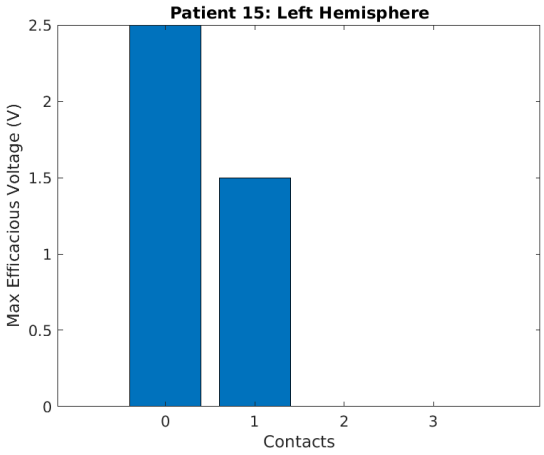
Patient 15: Left Hemisphere
Max Efficacious Voltage (V)
Contacts

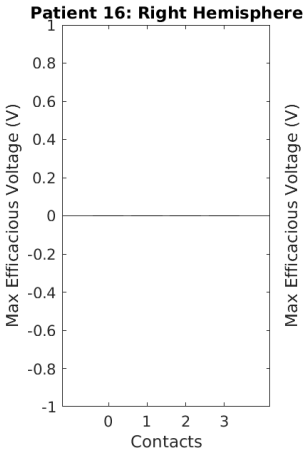
Patient 16: Right Hemisphere
Max Efficacious Voltage (V)
Contacts

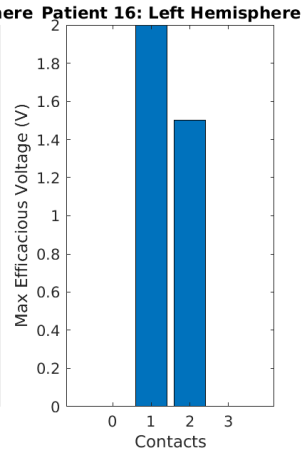
Patient 16: Left Hemisphere
Max Efficacious Voltage (V)
Contacts

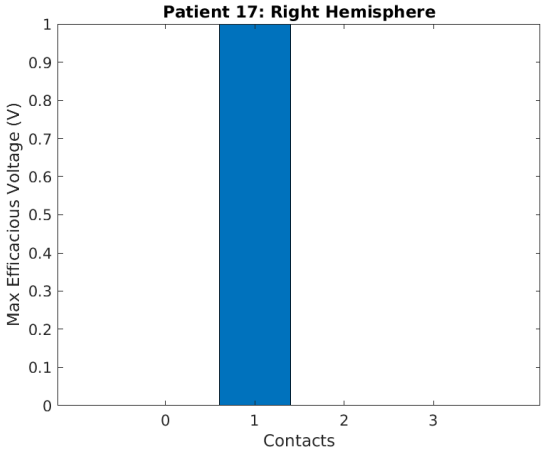
Patient 17: Right Hemisphere
Max Efficacious Voltage (V)
Contacts

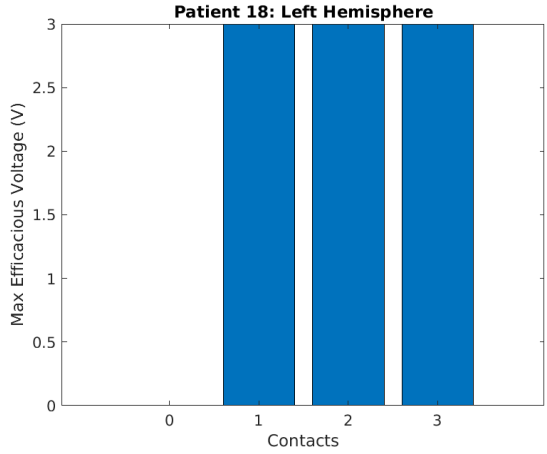
Patient 18: Left Hemisphere
Max Efficacious Voltage (V)
Contacts

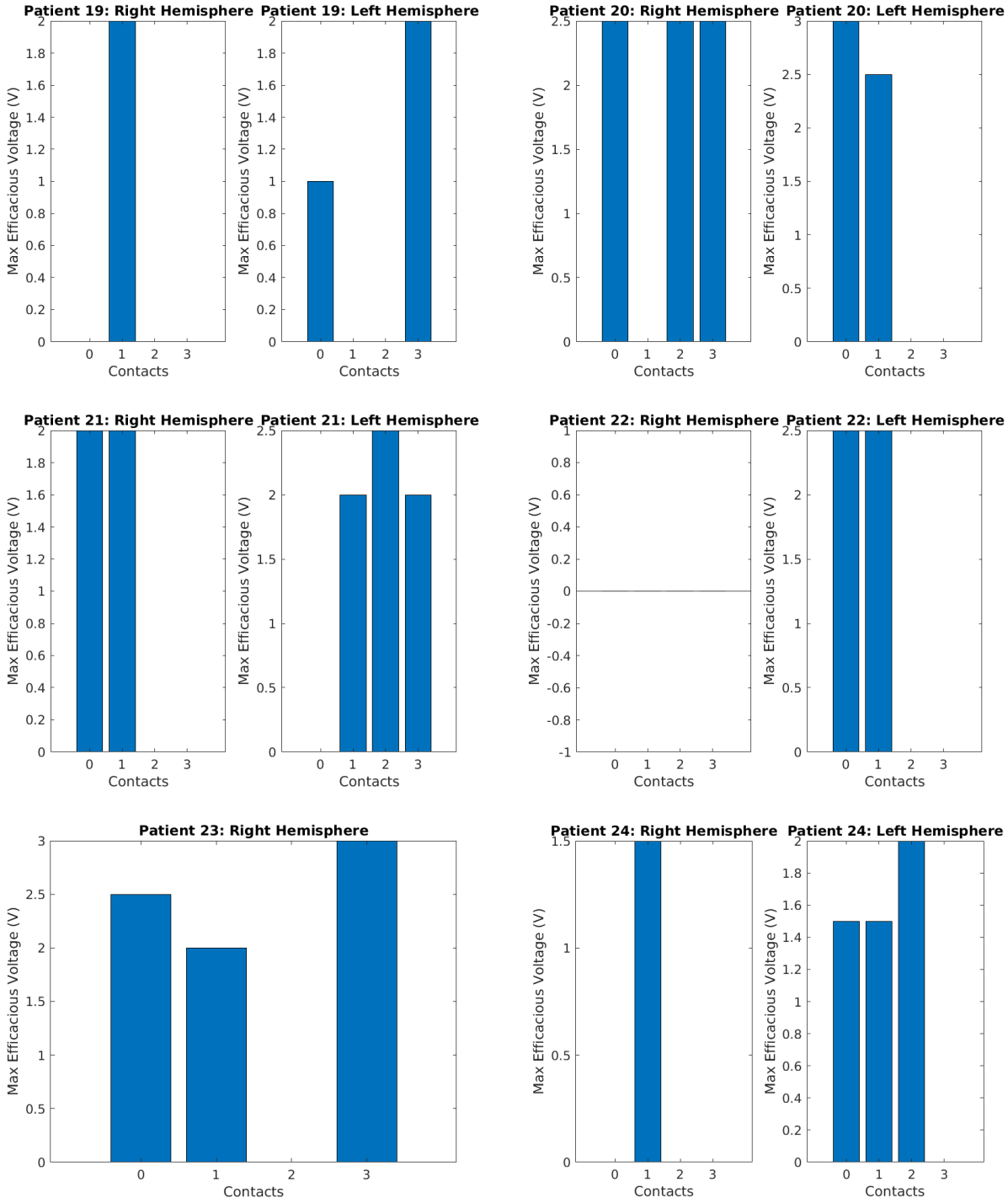

Figure 6: The highest efficacious voltage predicted at for each contact in each hemisphere for all 24 patients was predicted. This was then used to determine the most efficacious contact. Note that in some cases, no efficacious voltage was observed.

	Initial		1 Year		Final		Prediction	
Patients	**RH**	**LH**	**RH**	**LH**	**RH**	**LH**	**RH**	**LH**
1	3 2V	2 2 V	x	x	3 3 V	2 3 V	3 2 V	2 2.5 V
2	0, 2 3.5 V	1 1.5 V	0, 2 3.6 V	0, 1, 3 3.6 V	0, 2 3.6 V	0, 1 4.4 V	0, 1, 2 1.5 V	1, 2, 3 1.5 V
3	2 2 V	1 3 V	2 3.2 V	1 3.2 V	2 3.6 V	1 3.6 V	1 3.5 V	0, 3 3 V
4	-	0, 1 2.2 V	-	0, 1, 2, 3 3.6 V	-	0, 1, 2, 3 4.1 V	-	0, 1, 2 2 V
5	2 1.5 V	2 0.5 V	2 2.4 V	2 2.4 V	2 2.6 V	2 2.95 V	0, 1, 2, 3 0 V	0, 1, 2, 3 0 V
6	1 1 V	1, 2 3 V	2, 3 2.5 V	2, 3 2.7 V	3 2.4 V	2, 3 2.7 V	1, 2 1.5 V	0, 1, 2, 3 0 V
7	-	1 3.5 V	-	1 3.5 V	-	1 3.6 V	-	0, 1, 2, 3 0 V
8	-	0 1.5 V	-	0 1.5 V	-	0 1.5 V	-	1 3 V
9	1 2.3 V	1 2.4 V	1 2.3 V	1 2.1 V	1, 2 3.6 V	1, 2 3.5 V	3 2.5 V	0, 1 2 V
10	1, 2 1.8 V	1 1.6 V	1, 2 3.6 V	1, 2, 3 3 V	0, 1, 2 4 V	2, 3 3.6 V	0, 2 1.5 V	3 2 V
11	-	0, 1 3 V	-	1, 3 2 V	-	2, 3 2 V	-	2, 3 3 V
12	-	2 1.8 V	-	2 1.8 V	-	2 2 V	-	2 2 V
13	0 2.3 V	0 1.5 V	1, 3 2.6 V	0, 1 1.9 V	0, 1, 2 2.7 V	0, 1, 2 2.8 V	0, 2 2 V	1 2 V
14	-	1 2 V	-	2 2.8 V	-	2 2.5 V	-	3 3 V
15	-	2, 3 2.8 V	-	2, 3 2.8 V	-	2, 3 2.8 V	-	0 2.5 V
16	1, 2 1.5 V	2 2.5 V	x	x	2 1.7 V	2 2.5 V	0, 1, 2, 3 0 V	1 2 V
17	2 1 V	-	2 3.6 V	-	2 4 V	-	1 1 V	-

18	-	2, 3 3.5 V	-	3 2.9 V	-	3 2.5 V	-	1, 2, 3 3 V
19	0 1.5 V	1 2 V	2, 3 2.8 V	1 1.8 V	1, 3 2.5 V	1 2 V	1 2 V	3 2 V
20	1 1 V	2 1 V	1 2.9 V	2 2.6 V	1 2.2 V	2 3 V	0, 2, 3 2.5 V	0 2 V
21	1 2 V	2 2 V	1 2.5 V	2 2.5 V	2 2.4 V	2 2.5 V	0, 1 2 V	2 2.5 V
22	0 2 V	1 2 V	0, 2 3.6 V	1, 3 2 V	0, 3 3.6 V	1, 3 2.1 V	0, 1, 2, 3 0 V	0, 1 2.5 V
23	0 2.5 V	-	1, 3 2.6 V	-	1, 3 3.4 V	-	3 3 V	-
24	1 1 V	1, 2 1.7 V	1 1.4 V	1, 2 2.2 V	1 2.3 V	1, 2 2.5 V	1 1.5 V	2 2 V

Table 3: The prediction for the most efficacious contact and voltage for each hemisphere in each patient versus the final contact chosen after the initial, 1 year and final sessions is shown above. ("RH" = Right Hemisphere, "LH" = Left Hemisphere, "-" = lack of an implanted hemisphere and "x" = lack of data from that session.)

DISCUSSION

Justification of the Approach

In designing our approach, we first considered utilizing the location of stimulation to predict patient outcome. However, in a previous study by Nestor et al. (2014), it was found that the position and trajectory of the DBS lead relative to the mid-comissural point (MCP) alone was unable to reliable predict motor improvement. This finding is likely due to the fact that this approach fails to adequately accounts for the great neuroanatomical variability exhibited across patients (Nestor et al. 2014). Thus, it is also unlikely that anatomical location alone would be sufficient to predict the varied clinical outcomes observed during stimulation parameter titration. For this reason, we turned to a connectivity-based approach that could likely better adapt to differences in patient anatomy.

Analysis of the literature informed the potential validity of using a connectivity-based approach. Traditionally, there have been two competing explanations to improve the clinical efficacy of STN-DBS: 1) that stimulation deactivates neurons creating a sort of functional lesion and 2) that stimulation activates STN output neurons to "jam" errant activity in the basal ganglia-thalamocortical circuits (Carlson et al. 2010). However, in a study by Carlson et al. (2010), it was shown that DBS shifted firing in STN neurons towards more randomized patterns of activity, suggesting a modulation of brain networks in accordance with the latter hypothesis. Further research suggests that DBS modulates coupling between the STN and multiple, spatially-distinct areas of the cortex (Silberstein et al. 2005; Oswal et al. 2016). This has also been backed by more recent tractography-based studies, in which it has been found that DBS targets preferentially project to many of the same proposed network components (Koirala et al. 2016; Riva-Posse et al. 2018). However, the accuracy of tractography in determining local connectivity is potentially limited due to ambiguity introduced by fiber crossing (Maier-Hein et al. 2017). Finally, research also suggests that the networks modulated by DBS may be distinct to specific clinical domains, such as tremor, and may even be bilateral in nature (Timmermann et al. 2003; de Solages et al. 2010).

The previous research suggests that utilizing cortical connectivity to predict clinical outcome is a reasonable approach, as well as that it could be useful to segment the chosen cortical targets by hemisphere. In fact, the validity of a functional connectivity-based approach for modeling stimulation-induced network modulation and to predict neurostimulation strengths and targets has already been shown (Chen et al. 2017). Likewise, it has been shown that structural connectivity, using both whole-brain connectome and constrained tractography-based approaches, can be used to predict motor improvement (Horn and Kühn 2015; Akram et al. 2017). These studies suggest that the therapeutic effect of DBS is mediated through the modulated by a variety of regions within distinct motor networks. However, no study has to our knowledge aimed to study whole-brain structural connectivity using patient-specific tractography or utilized the connectivity associated with non-motor side effects. For this reason, we decided to take an unbiased approach, in which we would initially include connectivity to all regions.

However, because of the potential ambiguity of local connectivity, we chose to forgo the inclusion of the more local subcortical regions in this study, instead including only the more distal cortical regions derived from a cortical atlas. We then used reverse sequential feature selection to narrow down these regions to only to the most predictive cortical regions.

Selected Features

Though the number of narrowed-down, predictive features shown in Table 1 was relatively large, it was found upon sorting in Table 2 that the majority of the areas made up by these regions were associated with specific neurological functions, including motor (domains 1, 2, 3, 5, and 7), sensory (domain 4), visual (domains 8 and 15) or limbic (domain 6). This suggests that the accurate prediction of clinical outcome in Parkinson's requires information from a relatively large number of widely-distributed regions. This finding can be explained by the variety of clinical domains used in this study, which included both motor and non-motor effects, as well as the aforementioned findings that DBS modulates spatially-distributed networks in the brain (Silberstein et al. 2005; Oswal et al. 2016). However, further research is necessary to identify the relative importance of these regions in predicting clinical outcome, as well as their contribution to the prediction of individual clinical domains. By doing so, it would be possible to not only better understand the importance of these cortical regions in Parkinsonian dysfunction, but also to better tune the machine learning approach.

Prediction Results

While the overall classification error of 10.99% is relatively modest, it suggests that cortical connectivity changes are informationally useful for predicting the clinical outcome associated with specific DBS stimulation parameters. This is backed by the finding that these predictions can be used to predict the most efficacious contact with an average absolute deviation of 0.89, 1.17 and 1.08 contacts and 0.77, 1.10 and 1.21 V from the initial, 1 year and final stimulation parameter settings respectively. Though performance in contact and voltage prediction remains relatively stable, it does appear to decrease slightly over time. This may be due to the inclusion of only acute observations during stimulation

parameter titration, and, if so, it is likely that including observations from later sessions would increase performance of the algorithm in predicting contacts chronically. Additionally, it was found that 44.1% of the contacts predicted were non-efficacious with 6 leads being entirely non-efficacious. This suggests our algorithm could be used to eliminate a large number of contacts from stimulation parameter titration. However, as can be seen in Table 3, working settings were nonetheless found on the 6 entirely non-efficacious leads. This phenomenon may partially be explained by atypical connectivity patterns from these leads or non-ideal targeting locations, but requires further investigation. Together, these findings suggest the potential feasibility of personalized DBS parameter predictions tailored to individual patients, using patient-specific cortical connectivity derived from diffusion-weighted brain imaging.

In order to improve prediction performance, it is likely that further research will be necessary in both feature selection and machine learning approach. The number of cortical features is still rather large, and so it would be fruitful to investigate alternative feature selection methods to the one used in this study. Additionally, it is likely that the incorporation and/or substitution of alternative connectivity metrics, derived from alternative tractography techniques, subcortical connectivity, or even functional connectivity, could improve performance and minimize the number of features. Further, though the linear SVM approach used in this study was useful as a first-pass method to assess the utility of using our patient-specific cortical connectivity metric to predict clinical outcome, it is likely that more complex kernel-based methods or neural networks will be able to better to parse out the complex trends in cortical connectivity and with less features (Hofmann, Schölkopf, and Smola 2008; LeCun, Bengio, and Hinton 2015).

Finally, though our algorithm currently only predicts overall clinical outcome, it could be extended to the prediction of clinical outcome in specific clinical domains. By doing this, it will be possible not only to predict whether or not a given stimulation parameter combination will be efficacious, but also in what areas specifically the stimulation will lead to improvement or side effect. This could then be used in tandem with a relative weighting scheme, perhaps based on the number and types of improvement or side effect and their

severity or the strength of the voltage needed, to more robustly predict the voltage that will be most efficacious at each contact and to rank these contacts using a weighted efficacy score. These could then serve as starting points for stimulation parameter titration, greatly reducing the extent of parameter search.

CONCLUSION

This study is a useful first step towards the automation of stimulation parameter titration for DBS surgery. Specifically, we've proposed a patient-specific cortical connectivity metric using structural connectivity, as estimated by probabilistic tractography, from the site of stimulation to predict clinical outcome using a linear SVM. Our SVM achieved an overall classification error of 10.99% and average absolute contact and voltage deviation 0.89, 1.17 and 1.08 contacts and 0.77, 1.10 and 1.21 V from the initial, 1 year and final stimulation parameter settings respectively. Additionally, 44.1% of the contacts were found to be non-efficacious with 6 leads being entirely non-efficacious. Though these results are relatively modest, together they suggest that our metric is informative for predicting clinical outcome and narrowing down stimulation parameters. By refining our algorithm using more complex feature selection and machine learning methods and supplementing it with chronic observations and alternative connectivity metrics, we hope to improve performance considerably. Additionally, we hope to adapt our algorithm to predict the clinical domain(s) of the clinical outcome. By doing so, we will better be able to determine the maximally effective voltage at each contact, which can be used as a starting point for stimulation parameter titration. Ultimately, this will help to narrow down the parameter search space, saving time for both the patient and clinician and paving the way for the automation of stimulation parameter titration.

REFERENCES

Akram, Harith, Stamatios N. Sotiropoulos, Saad Jbabdi, Dejan Georgiev, Philipp Mahlknecht, Jonathan Hyam, Thomas Foltynie, et al. 2017. "Subthalamic Deep Brain Stimulation Sweet Spots and Hyperdirect Cortical Connectivity in Parkinson's Disease." *NeuroImage* 158 (September): 332–45. https://doi.org/10.1016/j.neuroimage.2017.07.012.

Anderson, Daria Nesterovich, Braxton Osting, Johannes Vorwerk, Alan D. Dorval, and Christopher R. Butson. 2018. "Optimized Programming Algorithm for Cylindrical and Directional Deep Brain Stimulation Electrodes." *Journal of Neural Engineering* 15 (2): 026005. https://doi.org/10.1088/1741-2552/aaa14b.

Assaf, Yaniv, and Ofer Pasternak. 2008. "Diffusion Tensor Imaging (DTI)-Based White Matter Mapping in Brain Research: A Review." *Journal of Molecular Neuroscience* 34 (1): 51–61. https://doi.org/10.1007/s12031-007-0029-0.

Buhlmann, Julia, Lorenz Hofmann, Peter Alexander Tass, and Christian Hauptmann. 2011. "Modeling of a Segmented Electrode for Desynchronizing Deep Brain Stimulation." *Frontiers in Neuroengineering* 4. https://doi.org/10.3389/fneng.2011.00015.

Carlson, Jonathan D., Daniel R. Cleary, Justin S. Cetas, Mary M. Heinricher, and Kim J. Burchiel. 2010. "Deep Brain Stimulation Does Not Silence Neurons in Subthalamic Nucleus in Parkinson's Patients." *Journal of Neurophysiology* 103 (2): 962–67. https://doi.org/10.1152/jn.00363.2009.

Chen, Xiaoyu, Chencheng Zhang, Yuxin Li, Pei Huang, Qian Lv, Wenwen Yu, Shengdi Chen, Bomin Sun, and Zheng Wang. 2017. "Resting-State Connectivity Predicts Patient-Specific Effects of Deep Brain Stimulation for Parkinson's Disease." *BioRxiv*, October, 203406. https://doi.org/10.1101/203406.

"Deep Brain Stimulation for Parkinson's Disease." 2018. The Lasker Foundation. 2018. http://www.laskerfoundation.org/awards/show/deep-brain-stimulation-for-parkinsons-disease/.

Fonov, Vladimir, Alan Evans, Robert Mckinstry, C.R. Almli, and Louis Collins. 2009. "Unbiased Nonlinear Average Age-Appropriate Brain Templates from Birth to Adulthood." *Neuroimage* 47 (July). https://doi.org/10.1016/S1053-8119(09)70884-5.

Glasser, Matthew F, Timothy S Coalson, Emma C Robinson, Carl D Hacker, John Harwell, Essa Yacoub, Kamil Ugurbil, et al. 2016. "A Multi-Modal Parcellation of Human Cerebral Cortex." *Nature* 536 (7615): 171–78. https://doi.org/10.1038/nature18933.

Hofmann, Thomas, Bernhard Schölkopf, and Alexander J. Smola. 2008. "Kernel Methods in Machine Learning." *The Annals of Statistics* 36 (3): 1171–1220. https://doi.org/10.1214/009053607000000677.

Horn, Andreas, and Andrea A. Kühn. 2015. "Lead-DBS: A Toolbox for Deep Brain Stimulation Electrode Localizations and Visualizations." *NeuroImage* 107 (February): 127–35. https://doi.org/10.1016/j.neuroimage.2014.12.002.

Jenkinson, Mark, Christian F. Beckmann, Timothy E. J. Behrens, Mark W. Woolrich, and Stephen M. Smith. 2012. "FSL." *NeuroImage*, 20 YEARS OF fMRI, 62 (2): 782–90. https://doi.org/10.1016/j.neuroimage.2011.09.015.

Kalia, Lorraine V., and Anthony E. Lang. 2015. "Parkinson's Disease." *The Lancet* 386 (9996): 896–912. https://doi.org/10.1016/S0140-6736(14)61393-3.

Koirala, N., V. Fleischer, O. Granert, G. Deuschl, M. Muthuraman, and S. Groppa. 2016. "Network Effects and Pathways in Deep Brain Stimulation in Parkinson's Disease." In *2016 38th Annual International Conference of the IEEE Engineering in Medicine and Biology Society (EMBC)*, 5533–36. https://doi.org/10.1109/EMBC.2016.7591980.

LeCun, Yann, Yoshua Bengio, and Geoffrey Hinton. 2015. "Deep Learning." *Nature* 521 (7553): 436–44. https://doi.org/10.1038/nature14539.

Maier-Hein, Klaus H., Peter F. Neher, Jean-Christophe Houde, Marc-Alexandre Côté, Eleftherios Garyfallidis, Jidan Zhong, Maxime Chamberland, et al. 2017. "The Challenge of Mapping the Human Connectome Based on Diffusion Tractography." *Nature Communications* 8 (November). https://doi.org/10.1038/s41467-017-01285-x.

"MATLAB - MathWorks." 2018. 2018. https://www.mathworks.com/products/matlab.html.

Miocinovic, Svjetlana, Suvarchala Somayajula, Shilpa Chitnis, and Jerrold L. Vitek. 2013. "History, Applications, and Mechanisms of Deep Brain Stimulation." *JAMA Neurology* 70 (2): 163–71. https://doi.org/10.1001/2013.jamaneurol.45.

Nestor, Kelsey A., Jacob D. Jones, Christopher R. Butson, Takashi Morishita, Charles E. Jacobson Iv, David A. Peace, Dennis Chen, Kelly D. Foote, and Michael S. Okun. 2014. "Coordinate-Based Lead Location Does Not Predict Parkinson's Disease Deep Brain Stimulation Outcome." *PLOS ONE* 9 (4): e93524. https://doi.org/10.1371/journal.pone.0093524.

Nowak, L. G., and J. Bullier. 1998. "Axons, but Not Cell Bodies, Are Activated by Electrical Stimulation in Cortical Gray Matter I. Evidence from Chronaxie Measurements." *Experimental Brain Research* 118 (4): 477–88. https://doi.org/10.1007/s002210050304.

Okun, Michael S., and Genko Oyama. 2013. "Mechanism of Action for Deep Brain Stimulation and Electrical Neuro-Network Modulation (ENM)." *Rinsho Shinkeigaku* 53 (9): 691–94. https://doi.org/10.5692/clinicalneurol.53.691.

Ondo, William G., Helen Bronte-Stewart, and DBS Study Group. 2005. "The North American Survey of Placement and Adjustment Strategies for Deep Brain Stimulation." *Stereotactic and Functional Neurosurgery* 83 (4): 142–47. https://doi.org/10.1159/000088654.

Oswal, Ashwini, Martijn Beudel, Ludvic Zrinzo, Patricia Limousin, Marwan Hariz, Tom Foltynie, Vladimir Litvak, and Peter Brown. 2016. "Deep Brain Stimulation Modulates Synchrony within Spatially and Spectrally Distinct Resting State Networks in Parkinson's Disease." *Brain* 139 (5): 1482–96. https://doi.org/10.1093/brain/aww048.

Picillo, Marina, Andres M. Lozano, Nancy Kou, Renato Puppi Munhoz, and Alfonso Fasano. 2016a. "Programming Deep Brain Stimulation for Parkinson's Disease: The Toronto Western Hospital Algorithms." *Brain Stimulation: Basic, Translational, and Clinical Research in Neuromodulation* 9 (3): 425–37. https://doi.org/10.1016/j.brs.2016.02.004.

Picillo, Marina, Andres M. Lozano, Nancy Kou, Renato Puppi Munhoz, and Alfonso Fasano. 2016b. "Programming Deep Brain Stimulation for Tremor and Dystonia: The Toronto Western Hospital Algorithms." *Brain Stimulation: Basic, Translational, and Clinical Research in Neuromodulation* 9 (3): 438–52. https://doi.org/10.1016/j.brs.2016.02.003.

Riva-Posse, P., K. S. Choi, P. E. Holtzheimer, A. L. Crowell, S. J. Garlow, J. K. Rajendra, C. C. McIntyre, R. E. Gross, and H. S. Mayberg. 2018. "A Connectomic Approach for Subcallosal Cingulate Deep Brain Stimulation Surgery: Prospective Targeting in Treatment-Resistant Depression." *Molecular Psychiatry* 23 (4): 843–49. https://doi.org/10.1038/mp.2017.59.

Salcedo-Sanz, S., J. L. Rojo-Álvarez, M. Martínez-Ramón, and G. Camps-Valls. 2014. "Support Vector Machines in Engineering: An Overview." *Wiley Interdisciplinary Reviews: Data Mining and Knowledge Discovery* 4 (3): 234–67. https://doi.org/10.1002/widm.1125.

Schuepbach, W.M.M., J. Rau, K. Knudsen, J. Volkmann, P. Krack, L. Timmermann, T.D. Hälbig, et al. 2013. "Neurostimulation for Parkinson's Disease with Early Motor Complications." *New England Journal of Medicine* 368 (7): 610–22. https://doi.org/10.1056/NEJMoa1205158.

Schüpbach, W. M. Michael, Stéphan Chabardes, Cordula Matthies, Claudio Pollo, Frank Steigerwald, Lars Timmermann, Veerle Visser Vandewalle, Jens Volkmann, and P. Richard Schuurman. 2017. "Directional Leads for Deep Brain Stimulation: Opportunities and Challenges." *Movement Disorders* 32 (10): 1371–75. https://doi.org/10.1002/mds.27096.

Silberstein, Paul, Alek Pogosyan, Andrea A. Kühn, Gary Hotton, Stephen Tisch, Andreas Kupsch, Patricia Dowsey-Limousin, Marwan I. Hariz, and Peter Brown. 2005. "Cortico-Cortical Coupling in Parkinson's Disease and Its Modulation by Therapy." *Brain* 128 (6): 1277–91. https://doi.org/10.1093/brain/awh480.

Solages, Camille de, Bruce C. Hill, Mandy Miller Koop, Jaimie M. Henderson, and Helen Bronte-Stewart. 2010. "Bilateral Symmetry and Coherence of Subthalamic Nuclei Beta Band Activity in Parkinson's Disease." *Experimental Neurology* 221 (1): 260–66. https://doi.org/10.1016/j.expneurol.2009.11.012.

Timmermann, Lars, Joachim Gross, Martin Dirks, Jens Volkmann, Hans-Joachim Freund, and Alfons Schnitzler. 2003. "The Cerebral Oscillatory Network of Parkinsonian Resting Tremor." *Brain* 126 (1): 199–212. https://doi.org/10.1093/brain/awg022.

Tromp, Do. 2009. "Diffusion Tensor Imaging 101." *Diffusion Imaging* (blog). May 1, 2009. http://www.diffusion-imaging.com/2009/05/diffusion-tensor-imaging-101.html.

Williams, Nolan R., Kelly D. Foote, and Michael S. Okun. 2014. "STN vs. GPi Deep Brain Stimulation: Translating the Rematch into Clinical Practice." *Movement Disorders Clinical Practice (Hoboken, N.J.)* 1 (1): 24–35. https://doi.org/10.1002/mdc3.12004.

Zhang, Jie. 2013. "The Cone Beam O-Arm Imaging System: Radiation Dose, Image Quality, and Clinical Applications." *Recent Patents on Medical Imaging* 3 (December): 103–10. https://doi.org/10.2174/22106847036661312110034O4.